2018 Second IEEE International Conference on Robotic Computing

A Comparison of Constant Curvature Forward Kinematics for Multisection Continuum Manipulators

Anant Chawla
Department of Mechanical Engineering
Clemson University
Clemson, SC 29634
Email: achawla@clemson.edu

Chase Frazelle and Ian Walker
Department of Electrical
and Computer Engineering
Clemson University
Clemson, SC 29634
Email: (cfrazel,iwalker)@clemson.edu

***Abstract*—Over the past few years, modeling of continuum robots has been the subject of considerable attention in the research community. In this paper, we compare a set of forward kinematic models developed for continuum robots, with the underlying assumption of piecewise constant curvature. A new approximate kinematic model based on phase and actuator length differences is also introduced for comparison. The comparative evaluation consists of computer simulation and physical experiments on a multisection continuum robotic manipulator, the OctArm. The experiments include both elongation and bending in 3D space. The comparative accuracy of the models is reported, along with relative numerical stability. Further conclusions are drawn on the applicability of the models to different real-world scenarios.**

I. Introduction

Interest in continuum robotics continues to grow rapidly. Continuum robots feature a continuous backbone and can bend at any point along their structure. Often they are viewed as ”invertebrate” robots as opposed to ”vertebrate” nature of traditional rigid-link robots [1]. Owing to their novel physical characteristics, novel and unique applications have been identified. Continuum robots have found their application in, and are well suited to, narrow and cluttered environments in comparison with highly structured industrial factory floors and work cells. Their inherent compliance and maneuverability enable applications which were previously not feasible for robotics, including search and rescue tasks, underwater inspection and repair, and, most notably, minimally invasive surgery [2], [3], [4].

From the perspective of computing, the emergence of continuum robots presents new and interesting challenges in robotics. Unlike traditional robots composed from rigid elements, which can only change shape at discrete points in their structure, continuum robots can, at least in theory, change shape at any point along their structure. This significantly complicates their modeling (motivating, for example, a move from discrete to continuum shape models), and, as we shall discuss, introduces significant algorithmic issues and practical problems related to the interplay between the algorithms modeling them and their physical structure.

The physical structure of continuum robots has been largely inspired by biological creatures, and researchers have attempted to imitate nature’s continuum examples such as octopus arms, mammalian and reptile tongues, and elephant trunks, to varying degrees of success [5], [6] [7]. The diversity of potential applications for continuum robots has led the emergence of various designs [8]. Tendon-based continuum designs, which consist of remotely actuated tendons routed along the backbone of the robot have been developed for space operations and surgical procedures. Designs which are intrinsically or locally actuated via some type of artificial muscle within the backbone have seen numerous realizations in the recent years. Some examples include the ”Octarm”, the ”European Octopus” and the ”Bionic Assistant”. These types of continuum robots have also been used for medical procedures such as endoscopic stitching, obesity treatment and colonoscopic insertion. Concentric-tube designs have shown significant progress in medical applications, specifically in minimally invasive surgery, with numerous surgical systems appearing in the commercial market [9]. An emerging class of continuum robots have controllable backbone stiffness. Stiffness regulation can be achieved with the help of either a suitable pneumatically actuated tube design, fluid-based actuation (magnetorheological or electrorheological), or through jamming of granular media. Regardless of the physical architecture, almost all continuum robots exhibit the property of constant curvature (constant curvature along the length of individual sections of the backbone), and hence, constant curvature modeling of continuum robots is of key importance in the field [1].

The field of theoretical continuum robot kinematics has grown rapidly along with the related hardware development, with a steadily increasing richness and diversity in theoretical models proposed [1]. These models, the subject of this paper, concentrate on constant curvature sections, as reviewed in the following paragraphs.

Several approaches have emerged addressing the challenge of kinematic modeling of continuum manipulators. In early work, [10], Hirose proposed biologically inspired serpenoid

0-7695-6370-8/18/31.00 ©2018 IEEE
DOI 10.1109/IRC.2018.00046

curves, mimicking snake locomotion. A modal approach was taken by Chirikjian and Burdick [11], where the authors describe the robot shape using easily formulable modal functions specified as the product of a Bessel function with sines and cosines. Gravagne and Walker [12] employed a similar approach but instead used wavelet decomposition. The discrepancy between the shapes achievable by the finite number of proposed model curves and those of the continuum robot's backbone curve limited the applicability of this approach. Perhaps the most commonly adopted approach to modeling constant curvature continuum robot kinematics to date is that of [2], which introduced models for forward and inverse kinematics. The result, by relating backbone shape to actuator variables, extends that obtained in [13] which used virtual rigid-link kinematics and conventional D-H parameters to relate backbone shape to task coordinates [1], [8], [14], [15], which in turn can be shown to produce the same results as the approach by Mochiyama and Suzuki [16], [17], [18] which treats the robot backbone as a curve in space, and utilizes Frenet-Serret frame floating along the curve to characterize it. However, all these models suffer from numerical (algorithmic, i.e. numerical instabilities at configurations where there is no corresponding physical limitation) singularities and demand special numerical treatment when close to straight (zero curvature) section configurations. In response to the above limitations, an alternative stable yet computationally intensive approach was presented by Godage et al. [3], [19] using mode shape functions, wherein the configuration space variables are approximated using multivariate Taylor series. This approach has until recently been established as the most numerically stable currently in the literature. However, recently a new singularity-free analytical approach for modeling constant curvature kinematics has been introduced [20]. Herein we compare this new approach with the mode shape approach in [3], and the commonly used approach of [2] and an approximation to it.

In other work in continuum kinematic modeling, the use of exponential coordinates to define kinematics has also appeared in the literature [14], [21], [22], and is shown to lead to essentially the same results as other constant curvature kinematic models. When assuming non-constant curvature, the theory of Cosserat Rods has been particularly useful in deriving geometrically exact kinematic models which account for external and gravitational loading, but are harder to implement and complex in nature [23], [24], [25].

This paper introduces a new approximate version of the kinematic model in [26], and compares it with prevalent constant curvature kinematic models with respect to its accuracy. The new approximate model relies on the linear and angular differences between actuator lengths to establish the configuration space variables.

The models analyzed and compared in this paper are [2], [3], [20] and the new approximate model, from here on referred as the Jones Model, Godage Model, Allen Model, and Walker-Frazelle Model, respectively. These algorithms are detailed in Section II. Experiment based comparison considering both spatial bending and elongation using the three section, nine degree of freedom OctArm continuum robot [2], [6] and supplemented with simulations is presented in Section III. Discussion and conclusions are presented in Sections IV and V, respectively.

II. Kinematic Models

A fundamental difference exists between the forward kinematics mapping for a conventional serial rigid link manipulator and a continuum manipulator. For traditional rigid link robots, a standard homogeneous transformation matrix T with variables ($\underline{\theta}$, $\underline{d}$) obtained via the Denavit-Hartenberg formulation transforms the local shape coordinates ($\underline{\theta}$, $\underline{d}$) into task space coordinates $\underline{x}$, representing the position and orientation of end-effector typically [2]. The transformation is straightforward due to finite number of joints and uses one independent variable per joint representing either a translation $\underline{d}$ or a rotation $\underline{\theta}$. On the other hand, continuum manipulators have a theoretically infinite number of joints leading to coupled rotational and translational motions along the backbone.

A. Jones Kinematic Model

As can be seen in Figure 1, the piecewise constant-curvature assumption affords decomposition of the mapping from actuator space q to task space x into two independent steps [8]. This model maps the actuator space coordinates q with the configuration space coordinates ($s(t)$, $\kappa(t)$, $\phi(t)$), where $s(t)$ is the arc length, $\kappa(t)$ represents curvature, and $\phi(t)$ is the bending plane angle in the frame attached to the base of the section. The homogeneous transformation matrix (HTM) A is given by (1), where c(ϕ) = cos(ϕ) and s($s\kappa$) = sin($s\kappa$).

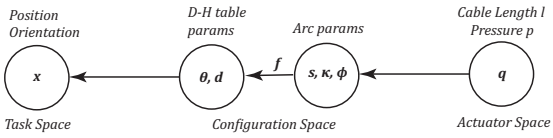

Fig. 1. Mapping from Actuator Space to Task Space

$$H(s,\kappa,\phi) = \begin{bmatrix} c(\phi) & -s(\phi)c(s\kappa) & s(\phi)s(s\kappa) & \frac{s(\phi)(1-c(s\kappa))}{\kappa} \\ s(\phi) & c(\phi)c(s\kappa) & -c(\phi)s(s\kappa) & \frac{-c(\phi)(1-c(s\kappa))}{\kappa} \\ 0 & s(s\kappa) & c(s\kappa) & \frac{s(s\kappa)}{\kappa} \\ 0 & 0 & 0 & 1 \end{bmatrix}, \quad (1)$$

Using purely geometrical means, the expressions for $s(t)$, $\kappa(t)$, and $\phi(t)$ are found out to be as follows, whose values are then substituted in equation 1 to obtain the final HTM. Note that the HTM given above is different from the one in [2] because it measures ϕ with respect to $-Y$ axis, and does not include the final rotation about Z axis for orientation at the tip section. This is achieved by subtracting ϕ of the proximal section by the immediately distal section, resulting in a more concise form.

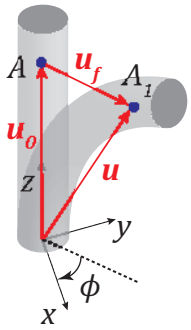

Fig. 2. Mapping from Actuator Space to Task Space

$$s = \frac{(l_1 + l_2 + l_3)nd}{\sqrt{l_1^2 + l_2^2 + l_3^2 - l_1 l_2 - l_2 l_3 - l_1 l_3}} \cdot \sin\left(\frac{\sqrt{l^2{}_1 + l^2{}_2 + l^2{}_3 - l_1 l_2 - l_2 l_3 - l_1 l_3}}{3nd}\right) \quad (2)$$

$$\kappa = 2\frac{\sqrt{l_1^2 + l_2^2 + l_3^2 - l_1 l_2 - l_2 l_3 - l_1 l_3}}{d(l_1 + l_2 + l_3)} \quad (3)$$

$$\phi = \tan^{-1}\left(\frac{\sqrt{3}}{3}\frac{l_3 + l_2 - 2l_2}{l_2 - l_3}\right) \quad (4)$$

B. Godage Kinematic Model

The Godage Model uses parameters $\{\lambda(t),\ \phi(t),\ \theta(t)\}$ to describe a point along the neutral axis of a continuum arm section. The parameter $\lambda(t)$ is the radius of curvature, $\phi(t)$ represents the elevation angle in section bending plane, and $\theta(t)$ is the angle subtended by the section bending plane with the $+X$ axis in the base frame. The key idea behind this model is given in (5), i.e. the displacement of any point on the continuum structure can be expressed in terms of multivariate Taylor series as the product of a vector of elastic coordinates ($\mathbf{q}_f$) and a shape matrix ($\mathbf{S}$) defined by coefficients. $\mathbf{q}$ is the joint variable vector of the section consisting of actuator lengths, $\mathbf{q}(t) = \{[l_1(t), l_2(t), l_3(t)]^T : \mathbf{q} \in \Re^{3x1}\}$. The scalar $\xi \in [0,\ 1]$ defines the points along the neutral axis where ξ = 0 is the section base. Figure 2 illustrates the concept where a point A on the neutral axis with $\mathbf{u}_0$ as the original position vector is displaced to A_1 after deformation [19].

$$\mathbf{u}_f(t, \xi, \mathbf{q}) = \mathbf{S}(\xi)\mathbf{q}_f(t, \mathbf{q}) \quad (5)$$

$$\mathbf{u}(t, \xi, \mathbf{q}) = \mathbf{u}_0(\xi) + \mathbf{S}(\xi)\mathbf{q}_f(t, \mathbf{q}) \quad (6)$$

Referring to Figure 3, for any given section i, a homogeneous transformation matrix (HTM) $\mathbf{T}$ is defined as

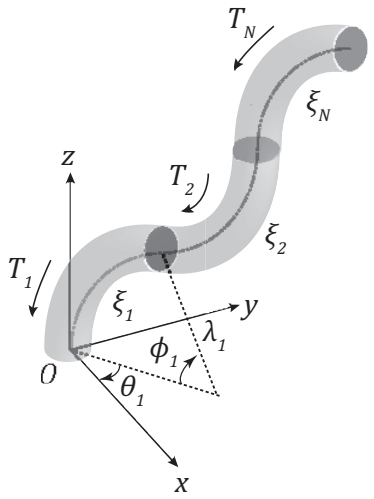

Fig. 3. Mapping from Actuator Space to Task Space

$$^{i}_{i-1}\mathbf{T}(\xi_i, \mathbf{q}_i) = \mathbf{R}_z(\theta_i)\mathbf{P}_x(\lambda_i)\mathbf{R}_y(\xi_i\phi_i)\mathbf{P}_x(-\lambda_i)\mathbf{R}_z^T(\theta_i) \quad (7)$$

$$= \begin{bmatrix} \mathbf{R}(\xi_i, \mathbf{q}_i) & \mathbf{p}(\xi, \mathbf{q}_i) \\ \mathbf{0}_{1x3} & 1 \end{bmatrix} \quad (8)$$

$$^{i}_{i-1}\mathbf{T}_\phi(\xi_i, \mathbf{q}_i) = \begin{bmatrix} \phi_R(\xi_i, \mathbf{q}_i) & \phi_P(\xi_i, \mathbf{q}_i) \\ \mathbf{0}_{1x3} & 1 \end{bmatrix} \quad (9)$$

where $\mathbf{R}_z$ and $\mathbf{R}_y$ are rotational matrices about the $\mathbf{Z}$ and $\mathbf{Y}$ axes, and $\mathbf{P}_x$ is the translation matrix along the $\mathbf{X}$ axis [3]. Since every element of the HTM is essentially a linear or angular displacement, the mode shape functions (MSFs) as given in 7 and 9 can be obtained for each element, resulting in a modal transformation matrix (MTM), $^{i}_{i-t}\mathbf{T}_\phi$, given in (8).

C. Allen Kinematic Model

The Allen model is first presented in [20]. Similar to the Jones and Godage models, the Allen model uses three parameters to describe a single continuum section in three dimensional space. The first two parameters, denoted $u(t)$ and $v(t)$, are part of a rotation vector $\omega(t) = [u(t), v(t), 0]^T$ that describes the orientation of the section's end frame relative to the section's base frame. The value $u(t)$ can be described as the rotation around the X-axis in the base frame and $v(t)$ describes the rotation about the Y-axis. The rotation component about the Z-axis is always zero. These values equate to a total rotation $\theta = \sqrt{u^2 + v^2}$ about the unit vector $\omega/\|\omega\|$. The third parameter is the section length, or arc length, as previously defined. We again use the variable $s(t)$ to denote the central length of the section.

The transformation matrix for the Allen model is given as:

$$H(u,v,s) = \begin{bmatrix} \gamma v^2 + 1 & -\gamma uv & \zeta v & -\gamma sv \\ -\gamma uv & \gamma u^2 + 1 & -\zeta u & \gamma su \\ -\zeta v & \zeta u & \cos(\theta) & \zeta s \\ 0 & 0 & 0 & 1 \end{bmatrix}, \quad (10)$$

where $\zeta(\theta) = \sin(\theta)/\theta$ and $\gamma(\theta) = (\cos(\theta) - 1)/\theta^2$. It can be shown that the functions $\zeta(\theta)$ and $\gamma(\theta)$ are still defined when θ is zero. The equations for calculating $u(t)$ and $v(t)$ for a three-tendon, 120° configuration manipulator are given in equations (11) and (12), respectively. These are derived by converting the four-tendon based equations presented in [20] to a three-tendon model.

$$u(t) = \frac{l_2 - l_3}{d\sqrt{3}} \quad (11)$$

$$v(t) = \frac{s(t) - l_1}{d} \quad (12)$$

The original reporting of the Allen model assumes a fixed value for $s(t)$. We cannot make this assumption, and therefore have chosen to calculate arc length using equation (13).

D. Walker-Frazelle Approximation Model

The Walker-Frazelle Model is an approximation of the Jones Model with the intent of low computational complexity and elimination of singularities. Consequently, this approach only introduces new approximate values for $s(t)$, $\kappa(t)$, and $\phi(t)$, with rest of the transformation and implementation remaining same. The expression for arc length ($s(t)$) is given as the average of the three cable lengths, seen in equation (13). Note that this value is accurate for pneumatic actuators which bend continuously, and for cable actuated robots in case of pure elongation (or contraction) [2].

$$s(t) = \frac{l_1 + l_2 + l_3}{3} \quad (13)$$

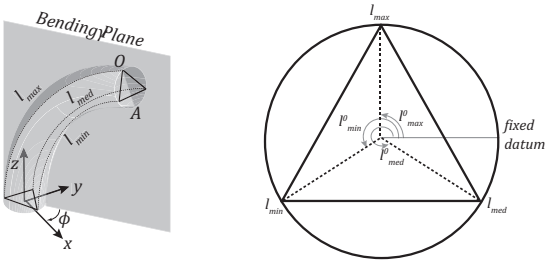

Fig. 4. Actuator Lengths Arranged Around Datum

The algorithm for calculation of $\phi(t)$ is given below. First, at any particular instant of time the actuator lengths l_1, l_2, l_3 are ordered on the basis of largest to smallest magnitude lmax, lmed, lmin, as shown in Figure 4. A datum is chosen at the top cross-section, with respect to which we measure angles subtended by different actuator lengths l^0max, l^0med, l^0min, all of which are fixed. Second, the algorithm calculates the relative difference between the actuator lengths and uses interpolation to get $\phi(t)$. Interpolation is the linear approximation employed in this case. When all the actuator lengths are of equal value implying a case of pure elongation (or contraction), $\phi(t)$ is undefined. The case of bending about one actuator is given by (10) and when two or more actuators are in operation, the value of $\phi(t)$ is given by (11). The value of α is 1 when, $l^0min = l^0max + \frac{2\pi}{3}$, and -1 when, l^0min = $l^0max - \frac{2\pi}{3}$.

$$\phi(t) = l^0_{max} + \pi \quad (14)$$

$$\phi(t) = l^0_{max} + \pi - \alpha\left(\frac{l_{med} - l_{min}}{l_{max} - l_{min}}\right) \quad (15)$$

The curvature $\kappa(t)$ expression is obtained by substituting the values of $s(t)$ and $\phi(t)$. Consider the case when a single section continuum arm bends at an angle ϕ with curvature κ and arc length s as shown in Figure 4. Let $\overline{OA}$ be the line at which the bending plane intersects with the top cross-section, and P and Q be two points on the line $\overline{OA}$ as shown in Figure 5. Let s_p and κ_p be the arc length and curvature at point P, and s_q and κ_q be the arc length and curvature at point Q. Since θ is constant,

$$s\kappa = s_p\kappa_p = s_q\kappa_q = \frac{\Delta s}{\Delta r} = \theta \quad (16)$$

where Δs = s_p - s_q and Δr is the length PQ found below. Let γ be the angle subtended by line $\overline{OA}$ with the line joining the minimum actuator length and center C, in this case RC. Thus, the $\angle SCP$ shown in Figure 5 is equal to $\frac{\pi}{3}$ - γ.

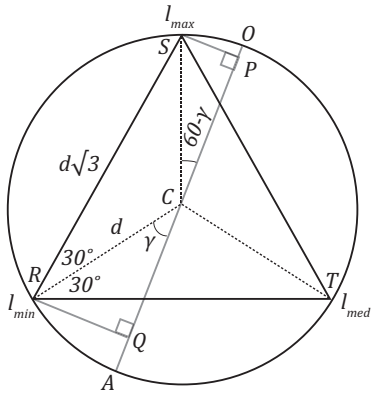

Fig. 5. Mapping from Actuator Space to Task Space

Utilizing trigonometric relations in triangles PSC and QRC, we get the value of Δr. The value of Δr and $s(t)$ is then substituted in equation (16) to obtain the value of $\kappa(t)$.

$$\Delta r = PC + CQ = d[\cos(\frac{\pi}{3} - \gamma) + \cos(\gamma)] \quad (17)$$

$$\kappa(t) = \frac{l_{max} - l_{min}}{\left(\frac{l_1 + l_2 + l_3}{3}\right) d[\cos(\frac{\pi}{3} - \gamma) + \cos(\gamma)]} \quad (18)$$

Due to the geometry of the physical build, the value of γ lies between 0 to $\frac{\pi}{3}$. The value for δs is taken as $l_{max} - l_{min}$ rather than actual since the difference is negligible.

III. Experimental Validation

The experimental trials include spatial bending and elongation on the OctArm to delineate the accuracy of the four models, namely Jones, Godage, Allen, and Walker-Frazelle Model, under various configurations. The measurement of the actual displacement is done with an ad-hoc calibrated aluminum framing system, shown in Figure 7 along with the OctArm. The set of trials were planned to be representative of the entire configuration space.

A. Implementation

The OctArm is a soft continuum manipulator which consists of three sections and nine degrees of freedom, each section with two axes bending and elongation. The motion in every section is achieved by circumferentially joining three or six pneumatically actuated McKibben muscles, regulated via pressure control valves. More details on the OctArm can be found in [2], [6], [27], [28] . The simulation model was implemented on Matlab 2011a.

Details of the experiments performed along with simulation results are as follows. A total set of 11 configurations were used, represented by their input pressure to each of the nine muscle groups of the OctArm. The configurations consist of 3 pure elongation configurations, 7 curved configurations, and a non-actuated case in order to observe any error inherently present in the models or system. An example of the system setup can be seen in Figure 6, which shows the unactuated OctArm and the aluminum frame measuring tool used to record actual end-effector locations for each experiment.

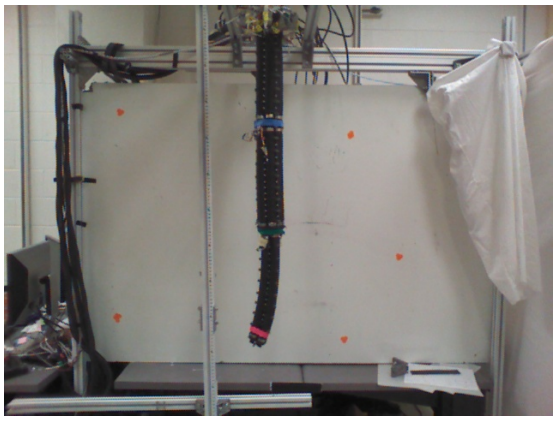

Fig. 6. Experimental setup for Kinematic Model Evaluation

Pure elongation motion is achieved by giving identical pressure to all three actuators of a section. The input pressures, measured in psi, for the 3 elongation configurations is given in Table I along with the input for the control case. The maximum input pressure for each of the pneumatic muscles is 90 psi.

Muscle	CFG 1 (psi)	CFG 2 (psi)	CFG 3 (psi)	CFG 4 (psi)
Base 1	0	0	65	52
Base 2	0	0	65	52
Base 3	0	0	65	52
Mid 1	0	52	0	52
Mid 2	0	52	0	52
Mid 3	0	52	0	52
Tip 1	0	0	39	52
Tip 2	0	0	39	52
Tip 3	0	0	39	52

TABLE I
Input Pressures for Configurations 1-4

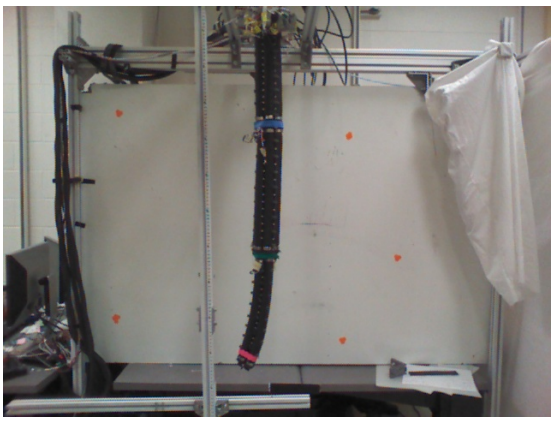

Fig. 7. Configuration 2: Mid Section Extension

Figure 7 depicts the OctArm in configuration 2, where the entire mid section is actuated at 52 psi.

Bending is achieved in a section by providing inputs to one or two actuators of the section, which might be of similar or differing value. The set of input pressures for the 7 curved configurations are seen in Table II. Figure 8 depicts configuration 8, with each of the three sections curving in a different plane.

Muscle	CFG5 (psi)	CFG6 (psi)	CFG7 (psi)	CFG8 (psi)	CFG9 (psi)	CFG10 (psi)	CFG11 (psi)
Base 1	0	78	0	22	0	0	0
Base 2	0	0	65	0	46	0	72
Base 3	0	78	65	78	46	59	0
Mid 1	0	0	0	0	46	0	52
Mid 2	0	0	52	78	0	0	0
Mid 3	0	0	52	78	46	59	52
Tip 1	0	0	0	22	46	59	0
Tip 2	78	78	39	78	46	0	78
Tip 3	0	0	39	0	0	0	0

TABLE II
Input Pressures for Configurations 5-11

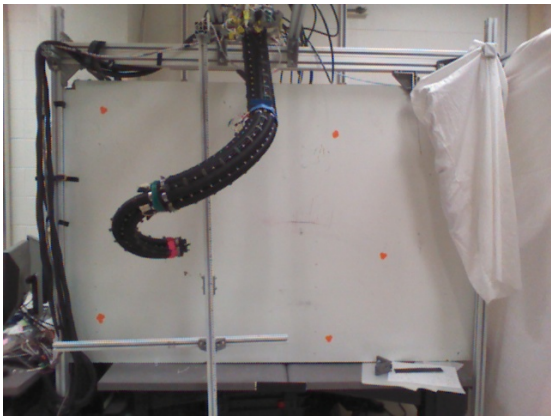

Fig. 8. Configuration 8: Three Section Non-planar Bending

IV. Experimental Results and Discussion

A. Model Comparison

Each model has its own pros and cons which consequently dictates its suitability. The Jones model and Allen model are geometrically exact approaches, while the Walker-Frazelle model and Godage model are approximations.

The Jones model's numerical requirement of non-zero section curvature introduces singularities and hence inaccurate results for purely extending motions. A limiting-case analysis for general class of continuum manipulators was presented by the authors to address this issue [26]. With respect to the experiments presented here, it was expected that the Jones model would perform best in the curved configurations and more poorly when measuring pure elongation.

The Godage Model is numerically stable at all configurations. Despite being a modal approach, the Godage model is computationally intensive. This is because the MSFs derived for every element of HTM need to be of fairly high degree in order to be a sufficiently accurate representation for all of configuration space.

The Allen model presents a mathematically stable solution while also reducing the complexity of implementation. Given the stability of the model, it was expected to perform well in both pure elongation and curved configurations.

The Walker-Frazelle Model is an approximate stable approach built upon the Jones Model. The intention of the model is to simplify mathematical complexity and remove the singularity presented by zero-curvature through the use of piece-wise continuous model. A distinction should be made that the enhanced stability in the Walker-Frazelle model comes at the cost of increased computational complexity.

B. Results

The results of the experimental trials as well as simulations are covered in this section. A comprehensive set of experiments were conducted so as to represent the entire configuration space. For example, in the case of the pure elongation, the experiments included an idle case with no input, actuation of a single section at a time, two sections at a time, and finally three sections, and with changing pressure inputs for every case. Extreme configurations, such as the one shown in Figure 8 were also included.

Model	CFG 1 [cm]	CFG 2-4 [cm]	CFG 5-11 [cm]	Total [cm]
Jones	3.5	5.3	6.8	6.3
WF Approx	3.3	5.0	8.0	7.1
Godage	3.6	2.7	13.1	9.9
Allen	3.5	5.3	6.8	6.3

TABLE III
Average Euclidean Error by Models

The accuracy of the four kinematic models across 11 configurations are reported in Table III. The errors are calculated as the euclidean error with respect to the manual measurements recorded for each configuration. The model errors in the control case are shown in column 2, the average model error for both the elongation and curved configurations are presented in columns 3 and 4, respectively. The total average error for all configurations is given in column 5.

As predicted, the Godage model did perform better, on average, than the other three models at approximating the end-effector location in purely elongation cases. However, the Godage model performed noticeably worse in all cases involving any amount of section curvature.

The Jones model and Allen model returned measurements that were identical for each of the test configurations. We tested several scenarios in order to separate these two models but were consistently met with the same result. While it was expected for the two models to perform on average better than the approximation models, it was not anticipated that the two models would return identical measurements for every test case. It was anticipated that the Allen approach would perform better than the Jones approach for configurations close to zero curvature. However, we were unable to find configurations for which this was the case. As can be seen, the two models were both several centimeters closer on average to the true value than either of the approximation models.

The Walker-Frazelle approximation on average performed better than the Godage approximation model but was inconsistent during configurations that tested the piece-wise nature of the approximation.

Given the results as presented, it is difficult to draw a clear victory for any singular model. When accounting purely for average error, the Jones and Allen models could be said to be equally reliable. Mathematically, the Jones model parameters involve more complex calculations and is unstable when approaching zero curvature. The Allen model is defined in the case of pure elongation and has relatively simple model parameter calculations.

V. Conclusion

A comparison of accuracy between four different forward kinematic models for multisection continuum robots is

presented. One of the models in comparison, the Walker-Frazelle model is introduced in this paper. The selected models cover a considerable spectrum of different constant-curvature kinematic approaches, such as modal, virtual rigid-link, and geometrically exact and approximate models.

Spatial bending and pure elongation experiments were conducted on the OctArm. The results indicate that there is no clear "best model", though the Jones and Allen models on average present the strongest case as geometrically exact constant curvature models. Contrary to our expectations, the Jones approach performed as well as, indeed identically to, the Allen method.

ACKNOWLEDGMENT

This work was supported in part by the U.S. National Science Foundation under grant IIS-1527165, in part by NASA under NRI contract NNX12AM01G, and in part by a NASA Space Technology Research Fellowship, contract 80NSSC17K0173.

REFERENCES

[1] I. Walker, "Continuous backbone "continuum" robot manipulators: A review," *ISRN Robotics*, vol. 2013, no. 1, pp. 1–19, Jul. 2013.

[2] B. Jones and I. Walker, "Kinematics for multisection continuum robots," *IEEE Trans. Robot.*, vol. 22, no. 1, pp. 43–57, Feb. 2006.

[3] I. Godage, E. Guglielmino, D. Branson, G. MedranoCerda, and D. Caldwell, "Novel modal approach for kinematics of multisection continuum arms," in *Proc. IEEE/RSJ Int. Conf. Intel. Robot. Syst.*, San Francisco, CA, 2011, pp. 1093–1098.

[4] Eelume. (2017, September) Eelume. [Online]. Available: https://eelume.com

[5] W. Kier and K. Smith, "Tongues, tentacles, and trunks: The biomechanics of movement in muscular hydrostats," *Zoological Journal of the Linnean Society*, vol. 83, no. 4, pp. 307–324, 1985.

[6] I. Walker, D. Dawson, T. Flash, F. Grasso, R. Hanlon, B. Hochner, W. Kier, C. Pagano, C. Rahn, and Q. Zhang, "Continuum robot arms inspired by cephalopods," in *Proc. SPIE Conf. Unmanned Ground Veh. Tech.*, Orlando, FL, 2005, pp. 303–314.

[7] D. Trivedi, C. Rahn, W. Kier, and I. Walker, "Soft robotics: Biological inspiration, state of the art, and future research," *Applied Bionics and Biomechanics*, vol. 5, no. 2, pp. 99–117, Jun. 2008.

[8] R. Webster III and B. A. Jones, "Design and kinematic modeling of constant curvature continuum robots," *Int. Jour. Robots. Res.*, vol. 29, no. 13, pp. 1661–1683, Jul. 2010.

[9] J. Burgner-Kars, D. C. Rucker, and H. Choset, "Continuum robots for medical applications: A survey," *IEEE Trans. Robot.*, vol. 31, no. 6, pp. 1261–1280, Dec. 2015.

[10] S. Hirose, *Biologically Inspired Robots*. Oxford, UK: Oxford University Press, 1993.

[11] G. Chirikjian and J. Burdick, "A modal approach to hyper-redundant manipulator kinematics," *IEEE Trans. Robot. Autom.*, vol. 10, no. 3, pp. 343–354, Jun. 1994.

[12] I. A. Gravagne, "Design, analysis and experimentation: the fundamentals of continuum robotic manipulators," Ph.D. dissertation, Clemson University, 2002.

[13] M. Hannan and I. Walker, "Analysis and experiments with an elephant's trunk robot," *Advanced Robotics*, vol. 15, no. 8, pp. 847–858, Aug. 2001.

[14] R. Murray, Z. Li, and S. Sastry, *A Mathematical Introduction to Robotic Manipulation*. Boca Raton, FL: CRC Press, 1993.

[15] M. W. Spong, S. Hutchinson, and M. Vidyasagar, *Robot Dynamics and Control*. New York, NY: John Wiley and Sons, 2005.

[16] H. Mochiyama and T. Suzuki, "Dynamic modeling of a hyper-flexible manipulator," in *Proc. SICE Annual Conf.*, Osaka, Japan, 2002, pp. 1505–1510.

[17] ——, "Kinematics and dynamics of a cable-like hyper-flexible manipulator," in *Proc. IEEE Int. Conf. Robot. Autom.*, Taipei, Taiwan, 2003, pp. 3672–3677.

[18] H. Mochiyama, "Whole-arm impedance of a serial-chain manipulator," in *Proc. IEEE Int. Conf. Robot. Autom.*, Seoul, Korea, 2001, pp. 2223–2228.

[19] I. Godage, D. Branson, E. Guglielmino, G. MedranoCerda, and D. Caldwell, "Shape function-based kinematics and dynamics for variable-length continuum robotic arms," in *Proc. IEEE Int. Conf. Robot. Autom.*, Shanghai, China, 2011, pp. 452–457.

[20] W. Felt, M. T. andT. Allen, G. Hein, J. Pompa, K. Albert, and D. Remy, "An inductance-based sensing system for bellows-driven continuum joints in soft robots," in *Robotics: Science and Systems*, The Hague, Netherlands, 07 2017.

[21] P. Sears and P. Dupont, "A steerable needle technology using curved concentric tubes," in *Proc. IEEE/RSJ Int. Conf. Intel. Robot. Syst.*, Beijing, 2006, pp. 2850–2856.

[22] R. J. Webster III, J. S. Kim, N. J. Cowan, G. S. Chirikjian, and A. M. Okamura, "Nonholonomic modeling of needle steering," *Int. Jour. Robots. Res.*, vol. 25, no. 5-6, pp. 509–525, Jul. 2006.

[23] D. Rucker and R. Webster III, "Deflection-based force sensing for continuum robots: A probabilistic approach," in *Proc. IEEE/RSJ Int. Conf. Intel. Robot. Syst.*, San Francisco, CA, 2011, pp. 3764–3769.

[24] D. Trivedi, A. Lofti, and C. Rahn, "Geometrically exact dynamic models for soft robotic manipulators," in *Proc. IEEE/RSJ Int. Conf. Intel. Robot. Syst.*, San Diego, CA, 2007, pp. 1497–1502.

[25] F. Renda and C. Laschi, "A general mechanical model for tendon-driven continuum manipulators," in *Proc. IEEE Int. Conf. Robot. Autom.*, St. Paul, Minnesota, 2012, pp. 3813–3818.

[26] B. A. Jones and I. D. Walker, "Limiting-case analysis of continuum trunk kinematics," in *Proc. IEEE Int. Conf. Robot. Auto.*, Rome, Italy, 2007, pp. 1363–1368.

[27] D. Trivedi, A. Lofti, and C. Rahnr, "Geometrically exact models for soft robotic manipulators," *IEEE Trans. on Robot.*, vol. 24, no. 4, pp. 773–780, Aug. 2008.

[28] D. Trivedi, D. Dienno, and C. Rahn, "Optinmal, model-based design of soft robotic manipulators," in *Proc. of ASME Int. Design. Eng. Tech. Conf.*, Las Vegas, NV, 2007.